Simulation studies of the faceting transition in a cubic Ising model

Loki Jörgenson and R. Harris
Department of Physics and Centre for the Physics of Materials, McGill University, Rutherford Building, 3600 University Street, Montréal, Québec, Canada H3A 2T8
(Received 12 November 1992)

The faceting transition of a crystal surface can be effectively simulated by a ferromagnetic Ising model on a simple-cubic lattice. In this paper, we study a planar interface in a fully three-dimensional Ising model, as well as an isolated bulk inclusion or droplet. We also demonstrate a method for identifying the faceting transition and compare it with the conventional techniques. Finally, we examine the effect of a driving force on the faceting transition of a droplet and the so-called *dynamic or kinetic roughening* of a moving planar interface. These results are compared with the current renormalization analysis of the faceting transition.

PACS number(s): 68.35.Bs; 82.65.Dp; 05.50.+q, 82.20.wt

I. INTRODUCTION

A stable interface between bulk phases has an equilibrium shape which is determined by thermodynamic considerations. On crystalline lattices, the equilibrium shape may demonstrate a structural transition at a critical temperature. Physically, this entails a transition from a faceted, highly correlated interface to a roughened, wandering interface; thermodynamically, it corresponds to the disappearance of the free energy of a crystal step and the divergence of the fluctuation correlation length. This phenomenon is referred to as the *roughening* or *faceting* transition.

In this paper we use a variation of the Creutz multidemon algorithm on a cubic Ising lattice to study the characteristics of the faceting transition via computer simulation. We simulate a planar {100} solid-liquid interface at equilibrium, a metastable solid droplet and an evaporating solid droplet suspended in a undercooled melt, and a planar {100} interface in the presence of a thermal gradient. The impact of geometry and external forces are investigated and compared with analytic expressions.

In Sec. II, we describe the computer model itself. We introduce enhancements which provide improved control of the thermal diffusion mechanism necessary for the dynamic processes. In Sec. III, we review the basic critical roughening theory and introduce an approach to characterize the interface. We then compare our simulation results with theory for the planar equilibrium interface. In Sec. IV, we examine the consequences of the geometry of a finite droplet on the transition. Noting the requirement of an external force to maintain metastability, we review the current renormalization results for this context and compare them to our simulations. In Sec. V, we study the relaxation and evaporation of a finite droplet when the stabilizing force is removed. Although there is no true faceting transition, we propose a mechanism to describe the transitionlike behavior that is observed. Finally in Sec. VI, we return to the planar interface and introduce a driving force via a weak thermal gradient. The *kinetic* faceting transition is observed and the results are compared with current dynamic descriptions.

II. THE SIMULATION MODEL

The simulation model has been discussed extensively elsewhere [1] both in the context of equilibrium and nonequilibrium problems. It has been shown to reliably model thermal diffusion processes involved in relaxation [2], steady states [3], and thermal instabilities [1,4]. Only the basic model will be outlined here, with specific attention to details relevant to the present study.

The system is an $L_x \times L_y \times L_z$ lattice of Ising spins, with $L_x = L_y$. The boundaries are maintained via a combination of periodic conditions and contact with a heat bath, depending on the particular requirements. The energy is defined by an Ising Hamiltonian

$$\mathcal{H} = -J \sum_{\langle i,j \rangle} s_i s_j - \Delta \sum_i s_i, \tag{1}$$

where the spins are $s_i = \pm 1$, $\sum_{\langle i,j \rangle}$ is over nearest neighbors, and Δ is a uniform external field. With Δ=0, this system has a second-order phase transition at $k_B T_c \simeq 4.512$ J [5], in units where the Boltzmann constant has been set to unity. Since the aim of this study is to examine the behavior of an interface, a degeneracy δ in the upper energy state is introduced, resulting in a system with a first-order phase transition at $T_m < T_c$, with a latent heat of transition λ of order 2Δ; the melting temperature T_m is defined by [6]

$$T_m = 2\Delta / \ln(\delta). \tag{2}$$

It can be set at any desired value by varying either Δ or δ. The presence of the external field and the spin degeneracy does not affect the faceting transition behavior of the model at coexistence; this is demonstrated in Sec. III where the planar case is compared favorably to established results.

The key feature of this model is that the coexistence temperature T_m is variable. This means that a stable, equilibrium interface is accessible at all temperatures, so that the roughening behavior intrinsic to the crystal structure can be fully investigated without undesirable nonequilibrium effects.

The dynamics of the system are controlled by a variant of the Creutz multidemon algorithm [7, 8]. An $L_x \times L_y \times L_z$ lattice of noninteracting demons has a one-to-one correspondence with the spins. Each demon carries a non-negative amount of energy ε_d. When a spin flip is attempted, the demon is interrogated: If the flip releases energy, it proceeds and the energy is given to the demon. If the flip requires energy and the demon has enough, it proceeds and the demon gives up the energy. Otherwise, the flip is inhibited. Initially, the demons are configured with a Boltzmann distribution of energies, since this is what is expected when there is thermal equilibrium with the spin system. During a Monte Carlo run, temperature in the neighborhood of a given spin is defined in terms of the distribution of demon energies in that immediate neighborhood $T \approx \bar{\varepsilon}_d$.

Although there is an inherent thermal diffusion in the Creutz algorithm, it is spin activated and thus the diffusion rate depends strongly on temperature. This makes controlling the diffusion process difficult and introduces problems with analysis. We therefore introduce an enhanced diffusion process which is independent of T and extremely flexible: Nearest-neighbor demons randomly exchange position via a Kawasaki-like exchange with no penalty. The diffusion constant D is thus related to the fraction of all the demons f_D which exchange per Monte Carlo step (MCS):

$$D = \frac{f_D}{4d},$$

where d is the dimensionality; f_D is of order unity and $d = 3$ for all results shown in this work. In comparison, the intrinsic diffusion process is sufficiently weak at all values of T that it can be ignored.

The spin system is configured in one of two initial states, either as a planar interface perpendicular to the $\hat{\mathbf{z}}$ direction between two bulk phases at (or near) coexistence (i.e., a simple *solid - liquid* interface) or as a *solid* inclusion within a undercooled *liquid* melt with the solid at T_m and the liquid at $T \leq T_m$. In the first case, the $z = 0$ and $z = L_z$ ends of the system are maintained at a constant temperature using a Metropolis algorithm, while the sides are periodic. In the second case, $L_x = L_y = L_z$ and all six sides are periodic and maintained at constant T. The phases are initialized with an average spin magnetization appropriate to the local temperature, using mean-field expressions for the bulk magnetization.

III. THE PLANAR INTERFACE AT EQUILIBRIUM

The faceting transition of the {100} interface of the three-dimensional (3D) Ising model is understood to be an infinite-order Kosterlitz-Thouless transition [9] with a characteristic temperature dependence of the step free energy, step-step correlation length, and interface width [10]. The behavior of the interface above and below the transition is not as well known; we describe it in terms of the surface's geometry and its thermal fluctuations.

A. Theory

The step free energy has been shown to be the dual conjugate of the inverse XY spin-spin correlation length [11], so that it goes to zero at T_R like

$$E_s = \begin{cases} E_o e^{-B/\sqrt{T_R - T}}, & T \to T_R- \\ 0, & T \geq T_R, \end{cases} \tag{3}$$

where B is a nonuniversal constant. The characteristic length for correlations between thermal fluctuations has been identified as the dual conjugate of the vortex-vortex correlation length in the XY model [12], and near T_R diverges like

$$\xi = \begin{cases} \xi_o e^{B/\sqrt{T_R - T}}, & T \to T_R- \\ \infty, & T \geq T_R; \end{cases} \tag{4}$$

here, B is the same nonuniversal constant as before. Similarly, based upon the height-height correlation function near T_R [12], the mean-square width increases like

$$\langle w^2(T) \rangle \propto C + 1/\sqrt{T_R - T}, \quad T \to T_R- \tag{5}$$

where C is a constant. Note that there is no explicit finite-size dependence in (5); this expression applies to systems of size $L > \xi(T)$. When $L < \xi(T)$, the interface appears as if it were roughened.

Above T_R, for a finite $L_x \times L_y \times L_z$ system, $\langle w^2 \rangle$ varies with L $(= L_x = L_y)$ and T like

$$\langle w^2(L,T) \rangle \propto \ln(L)(1/\pi^2 + C\sqrt{T - T_R}), \quad T \to T_R+ \tag{6}$$

where C is a nonuniversal constant. This behavior of $\langle w^2 \rangle$ has been observed in computer simulations and used to identify the transition temperature for the 3D Ising model as [13]

$$T_R/T_c \simeq 0.542 \pm 0.002.$$

This is consistent with analytic approaches [14, 15] which predict

$$T_R/T_c \simeq 0.546 \pm 0.004.$$

The interface can also be characterized away from the transition region. At temperatures above T_R, we know [16] that the width varies as

$$\langle w^2(L,T) \rangle \propto \frac{\ln(L)\, T}{\gamma(T)}, \quad T > T_R. \tag{7}$$

The factor T in this expression does not appear in Eq. (6) because, compared to $\sqrt{T - T_R}$, it is approximately

constant near T_R.

For present purposes, it is important to note that at $T < T_R$, $\langle w^2 \rangle$ is a single averaged aspect of a more fundamental quantity, the fluctuation probability density P_f. Analysis of this distribution provides a more reliable measure of the faceting transition, with better statistics, than other approaches in the literature. We define it in terms of a faceted reference plane, upon which there is a collection of *microfacets* which reflect the stochastic balance between the available thermal energy and the free-energy cost of forming a facet step. A microfacet is a small *island* on the interface which is one lattice constant higher than the reference plane and has a characteristic size l; it is equivalent to a nucleation site in a 2D system. At a given temperature T, the distribution of microfacet sizes is Boltzmann-like

$$P_f(l,T) = \Omega e^{-E_f(l)/T};$$

$E_f(l)$ is the free energy of a facet of size l , given by

$$E_f(l) = 4lE_s(T) - al^2 \triangle E_b(T),$$

assuming the site is square to first approximation (i.e., small and on a cubic lattice) and far from any other site. Here, $\triangle E_b$ is the bulk free-energy difference and a is the lattice constant. If the interface is assumed to be at coexistence (i.e., $\triangle E_b = 0$), the condition $\int_1^\infty P_f(l,T)dl \equiv 1$ defines the prefactor to be

$$\Omega = \frac{4E_s}{T} e^{4E_s/T}.$$

Note that the lower limit of the integral is unity; this reflects the discrete nature of the lattice which cannot support a microfacet of a size smaller than $l = 1$. The distribution $P_f(\ell, T)$ then measures the relative probability of a given size of microfacet appearing on an interface of infinite extent.

The mean microfacet area $\langle A \rangle$ is then

$$\begin{aligned} \langle A(T) \rangle &= \int_1^\infty l^2 \, P_f(l,T) dl \\ &= 1 + \frac{T}{2E_s}\left(1 + \frac{T}{4E_s}\right). \end{aligned} \tag{8}$$

Thus as E_s goes to zero at T_R (3), the mean facet area diverges strongly to infinity. This behavior was anticipated by Weeks and Gilmer [17] from a visual inspection of Monte Carlo simulations of a flat interface.

Similarly, the variance σ^2, which measures the dispersion of the microfacet area around $\langle A \rangle$, is

$$\begin{aligned} \sigma^2(T) &= \int_1^\infty (l^4 - \langle A \rangle^2) \, P_f(l,T) dl \\ &= 6\left(\frac{T}{4E_s}\right)^2 + 16\left(\frac{T}{4E_s}\right)^3 + 20\left(\frac{T}{4E_s}\right)^4, \end{aligned}$$

$$T < T_R \tag{9}$$

and the uncovered fraction A_0 of the reference plane, which by definition, goes to zero as $T \to T_R-$, becomes

$$A_0 = 1 - C\frac{T}{4E_s}\left(1 + \frac{T}{4E_s}\right), \tag{10}$$

where C is a constant which is model dependent. In the same regime, the interface width is proportional to the fraction of the surface covered by microfacets,

$$\langle w^2(T) \rangle \propto (1 - \langle A_0 \rangle)^2 \tag{11}$$

an expression which is consistent with (5) in the limit $T \to T_R-$.

As $T \to T_R-$, microfacets begin to overlap, corrections to Eqs. (8)–(10) for step-step interactions become important, and the simple microfacet description would seem to be less useful. However, it can be used quite close to T_R, since the essential physics is captured by the abrupt manner in which E_s goes to zero. Indeed, near T_R, the description is consistent with the established relationship between the thermal correlation length and E_s as expressed by Eqs. (3) and (4). To see this, we identify the mean facet size $\langle l \rangle$ as a measure of the correlation length, so that

$$\xi \propto \langle l \rangle = 1 + \frac{T}{4E_s}; \tag{12}$$

note that in the thermodynamic limit of infinitesimal fluctuations (i.e., using $\int_0^\infty$ instead of $\int_1^\infty$), we recover the form of the Fisher relation for the square Ising lattice [18], $\xi = T/\gamma_{2D}$ where the 2D surface energy corresponds to the step-free energy $\gamma_{2D} \sim E_s$. Since analytic results are available for E_s of the 3D Ising model [14], this expression also provides a useful description of ξ when $T < T_R$.

Above T_R, the crystal surface is no longer faceted. However, the microfacet distribution can still be defined via a geometric analysis, and the mean facet area $\langle A \rangle$ can be related to the mean curvature $\bar{\kappa}$, so that

$$\langle A \rangle \propto 1/\bar{\kappa} \propto T^{-1/2}, \quad T > T_R. \tag{13}$$

Details of this relation are given in the Appendix.

B. Results

To examine the behavior of an equilibrium planar interface of {100} orientation at coexistence, the coexistence temperature was varied over $T \equiv T_m \in [0.2T_c, 0.8T_c]$ through the external field via (2); the spin degeneracy was maintained at $\delta = 2$ for all runs. During the simulation, the interface was permitted to fully relax, requiring approximately 1000 MCS. The statistics were based on the final state of one to six runs, depending upon the proximity of T_m to T_R and upon lattice size L; larger systems required only one run to provide useful statistics. Lattice sizes were varied, $L \in [32, 512]$, with the system height held at a constant $L_z = 24$; this was sufficient to permit the largest systems at the highest T to relax to a fully roughened state without encountering the upper and lower boundaries. Figure 1 shows a series of equilibrium planar interfaces at temperatures above

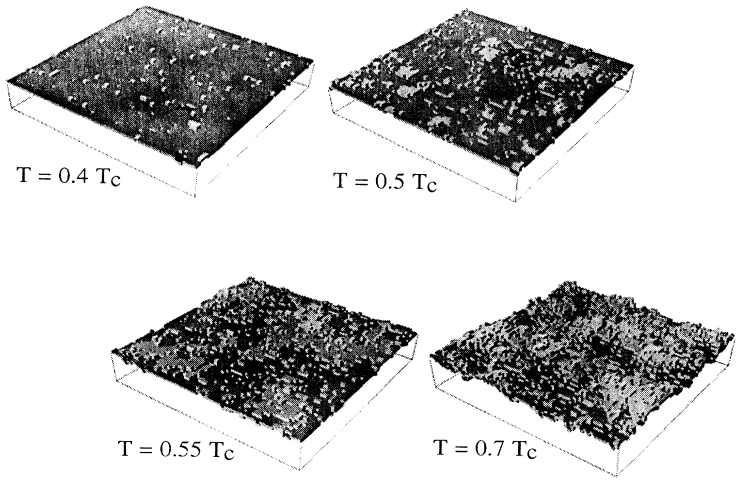

FIG. 1. Equilibrium planar interfaces for a 64 × 64 × 24 system at $T = 0.4T_c, 0.5T_c, 0.55T_c$, and $0.7T_c$. The lighter grey indicates higher surface level.

and below T_R.

In order to make contact with previous studies [13] and the analytic predictions (5)–(7) and (11), the width of the interface $\langle w(T)^2 \rangle$ was measured. This is defined as the mean-square width of a single-valued surface which is derived from the actual interface by elimiating all overhangs and bulk fluctuations. At most temperatures of interest, this is a very good approximation. Figure 2 shows $\langle w^2 \rangle$ for various L over a range of T: Away from $T_R \simeq 0.545T_c$ [14], the data follow both (7) and (11) in a credible manner, and near T_R are consistent with (5) and (6) (see inset) although too sparse to confirm them in detail. The data are similar to that of a recent study by Mon, Landau, and Stauffer [13] for systems of comparable size, in that finite-size effects are not very pronounced. From the position and sharpness of the cusp in the data, the faceting transition is estimated to be $T_R/T_c \simeq 0.54 \pm 0.01$; this can be improved by producing more data points with better statistics near the critical region, using the critical expressions for the width for analysis as did Mon, Landau, and Stauffer.

However, the analysis of the facet-size distribution displays the transition much more clearly using the same data. Figures 3 and 4 show $\langle A \rangle$ and σ^2. Their behavior is divergent near T_R and shows a distinct finite-size scaling at and above the transition, with σ^2 most clearly indicating the transition. Examining the divergence in the data, the transition temperature is estimated to be $T_R/T_c \simeq 0.542 \pm 0.005$. The expressions (8) and (9) are in good agreement with the data, using the low-T expansion for $E_s(T)$ of the 3D Ising model from Holzer and Wortis [14]. Above T_R, $\langle A(T) \rangle$ is expected to follow $T^{-1/2}$ (13); our results are consistent with this prediction, although the power law is too weak to fit unambiguously to the limited range of data.

In Fig. 5 we show the normalized area of the reference plane A_0. The data display a clear point of inflection near the anticipated T_R; from this, we estimate $T_R/T_c \simeq 0.542 \pm 0.008$. For the largest system (L=512), the data

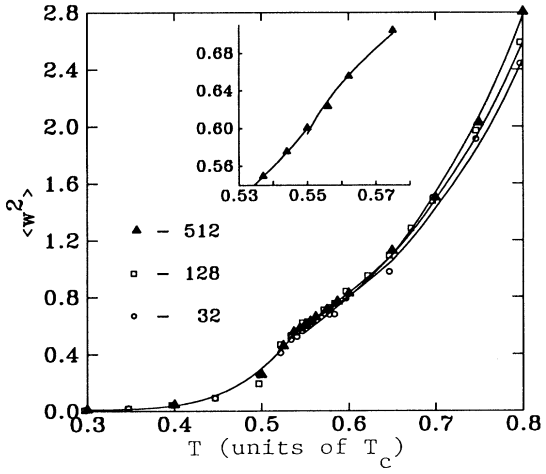

FIG. 2. The mean-squared width $\langle w^2 \rangle$ of the equilibrium planar interface at $T \in [0.3T_c, 0.8T_c]$ for system sizes $L = 32, 128$, and 512. The solid lines are the analytic expressions (11) and (7); note the finite-size dependence of the data above T_R. The inset shows the data near T_R with the solid lines being the expressions (5) and (6).

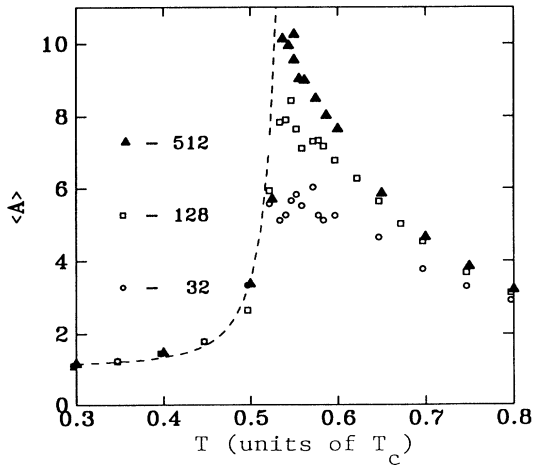

FIG. 3. The fractional area A_0 of exposed reference plane for an equilbrium planar interface at $T \in [0.3T_c, 0.8T_c]$ for system sizes $L = 32, 128$, and 512. The dashed line is the analytic expression (10) for $L = \infty$.

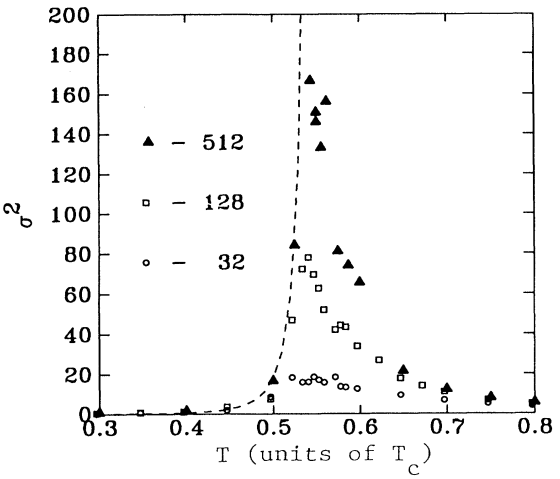

FIG. 4. The mean microfacet area $\langle A \rangle$ for the equilibrium planar interface at $T \in [0.3T_c, 0.8T_c]$ for system sizes $L = 32, 128$, and 512. The dashed line is the analytic expression (8).

agree well with (10), again using the expansion expression for $E_s(T)$.

IV. THE METASTABLE DROPLET AT EQUILIBRIUM

When the solid-liquid interface bounds a finite droplet instead of an infinite plane, all possible surface orientations are present. Below the faceting transition, the {100} reference plane manifests itself as six *macrofacets* with {100} orientation on a roughly cubical equilibrium crystal shape, with the macrofacets joined by curved, roughened surface. Equilibrium transition behavior is not strictly observable on such a droplet because, at coexistence, it is not stable; the system will tend to minimize the energy contribution of the interface by reducing the surface area and evaporating the droplet away. A unique counterforce F is required to balance the surface tension and provide a metastable interface; the equilibrium faceting transition is modified by the presence of this force [19].

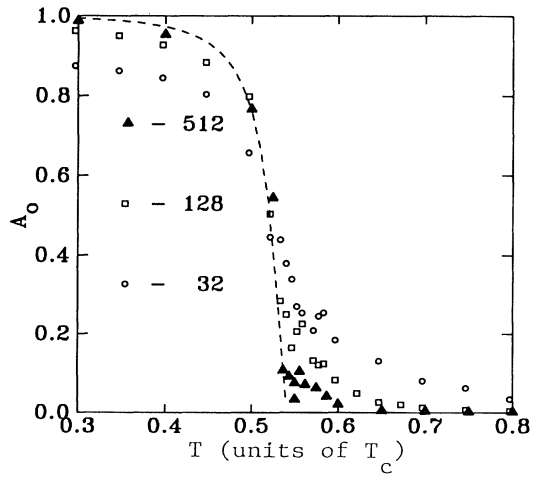

FIG. 5. The variance σ^2 of the mean microfacet area for the equilibrium planar interface at $T \in [0.3T_c, 0.8T_c]$ for system sizes $L = 32, 128$, and 512. The dashed line is the analytic expression (9).

A. Theory

Consider the free energy of a spherical droplet of radius R:

$$E_F = 4\pi R^2\gamma - \frac{4}{3}\pi R^3 \triangle E_b,$$

where $\triangle E_b$ is the bulk free-energy difference and γ is the surface energy. There is a metastable point where $dE_F/dR = 0$ at the critical radius

$$R^* = \frac{2\gamma}{\triangle E_b}.$$

When $R > R^*$, the droplet will tend to grow, and when $R < R^*$, the droplet will tend to shrink. At coexistence, when $\triangle E_b \equiv 0$, R^* becomes infinite, and all sizes of droplet will shrink. In order to study the faceting transition of a finite droplet at equilibrium, there must be a finite bulk free-energy difference $\triangle E_b$. There will only be a static interface in the presence of a driving force or *overpressure* $F \propto \triangle E_b$. The effect of this force on the faceting transition is that the T_R^* of the finite droplet interface is depressed below the transition temperature of the planar interface; as well, the transition behavior is spread over a greater range of T. Neither curvature nor finite-size effects can be suggested as the origin of this behavior; they may influence the scaling of the critical behavior but not the critical temperature itself.

For a static, faceted interface at temperature T, Nozières and Gallet [19] predict that a characteristic force F^* is required to shift the faceting transition to $T_R^* < T_R$ such that the interface *appears to be rough*:

$$F^*(T_R^*) = \gamma a/\xi^2 = E_s^2 a^3/\gamma, \tag{14}$$

where $\xi(T)$ is the step correlation length and a is the lattice constant. This expression can be compared to our data using values from analytic sources [14] for E_s and γ.

Visual inspection of the equilibrium crystal shape (ECS) shows a distinct dependence on T (see Fig. 6). The droplet is exactly cubic at $T = 0$; the corners become rounded as T increases; the faceted faces of the cube are circular and shrink as T approaches T_R; the macrofacets disappear completely at T_R, leaving only a roughened surface. Finally, as T approaches T_c and the surface tension becomes isotropic, the cuboid becomes spherical. It has been noted that the surface of a finite crystal can be mapped onto a two-phase system [20], with the curved, roughened portions of the surface representing one phase and the flat, faceted regions representing the other. The edges of the macrofacets below T_R are then phase boundaries and their size and shape correspond to the equilibrium crystal shape of a 2D droplet; this shape has been well defined theoretically for the nearest-neighbour 2D

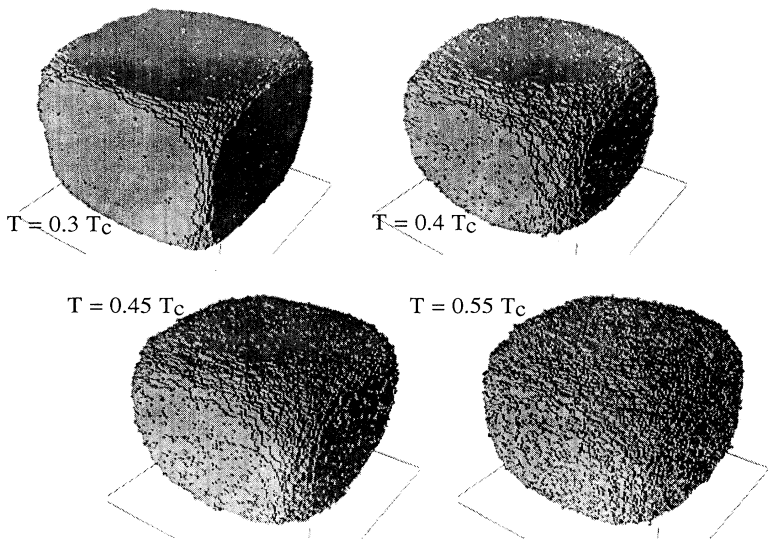

FIG. 6. Metastable interfaces for droplets of size 96^3 in a 128^3 system at temperatures $T = 0.3T_c, 0.4T_c, 0.45T_c$ and $0.55T_c$, near the modified faceting transition temperature $T_R^* \approx 0.45T_c$.

Ising model [21, 22]. The radius of the approximately circular face has been defined analytically through perturbative expansion as a function of T [22]; the inset in Fig. 7 shows the analytic normalized facet radius $r_f(T)$ as a function of temperature for directions parallel and diagonal to the Cartesian axes.

B. Results

To study the metastable droplets, we choose to look at an $L \times L \times L$ system with a droplet of size $\ell \times \ell \times \ell$ where $\ell = 0.75L$. The system parameters are chosen to satisfy metastability (i.e., $R \approx R^*$), and the overpressure required to maintain metastability F^* is provided by a bulk free-energy difference resulting from setting T_m slightly

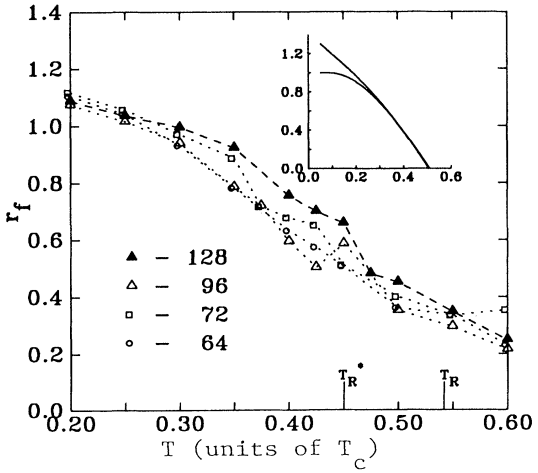

FIG. 7. The average macrofacet radius r_f for the metastable droplet as a function of temperature T for system sizes $L = 64, 72, 96$, and 128; the modified faceting temperature T_R^* is indicated. The inset shows the analytic prediction for r_f for an infinite droplet; the two lines are for r_f parallel and diagonal to the lattice axes.

higher than the ambient simulation temperature T. No exact prediction for F^* is available for a nonspherical droplet; consequently, the parameters are chosen empirically such that the droplet is metastable after quickly relaxing from a $T = 0$ cube to local equilibrium. If the droplet were not metastable, it would then begin to decay or grow. Above T_R, the metastable parameters are unique to within the amplitude of thermal fluctuations. Below T_R, the choice is complicated by exceedingly long time scales for the evaporation of an unstable, faceted interface; this is discussed in greater detail in Sec. V. The consequence is that our results well below T_R may be only *near* equilibrium. On the other hand, the results nearest to T_R are very precise and the correct transition behavior is preserved.

The droplet was initialized as a cube (ECS for $T = 0$) and allowed to relax to equilibrium for 5000–30 000 Monte Carlo steps. The trial temperatures ranged from $T \in [0.2T_c, 0.8\ T_c]$ for system sizes $L \in [32, 128]$. The largest contiguous facet on each of the six faces of the cube is identified with the anticipated macrofacet. The macrofacet radius r_f is based on the average area of the six largest facets $\bar{A}_f$ and the assumption that they are approximately circular (i.e., $\pi r_f^2 \equiv \bar{A}_f$). In addition, the microfacet size distribution for the entire surface is analyzed in a manner similar to the planar interface. (To make an exact comparison to the planar case, it would be necessary to isolate the microfacets on the macrofacets only. We judge the additional computational complexity not to be worthwhile.) Similarly, due to the inherent difficulty in defining the local width of a nonplanar surface, $\langle w^2 \rangle$ is not measured. Figure 6 shows a series of metastable droplets above and below the effective faceting temperature T_R^*.

The macrofacet area was taken from the average of the largest contiguous facets on each of the six faces of the droplet. Assuming the macrofacet shape to be circular, Fig. 7 shows the average macrofacet radius as a function of temperature; it has been normalized to the droplet radius, defined to be from the droplet center to the {100}

face. The transition point is less apparent than in the planar case; this is consistent with the predicted blurring of the roughening transition. If the inflection point is taken to be the transition point, T_R^* would be well below the equilibrium T_R, as expected. Alone this information is not very useful. However, it is more or less consistent with the expected form of $r_f(T)$ (see inset of Fig. 7).

The variance σ^2 shows the transition much more clearly as seen in Fig. 8; $\langle A \rangle$, shown for L=128 as an inset, is not a useful quantity at least with the limited statistics provided by our simulations. However, σ^2 indicates the transition distinctly at $T_R^*(\mathrm{L}{=}128)/T_c = 0.450 \pm 0.008$, well below the equilibrium transition temperature $T_R(\infty) \simeq 0.545 T_c$. A weak dependence on L is discernible in both the strength of the divergence and the shift in T_R, consistent with the increase in the necessary overpressure with decreasing system size.

Ideally the overpressure should be varied through a range of values for a single trial temperature T in order to identify the critical $F^*(T)$ which induces roughening. However, for any given system size L, there is only one F^* at a given T which results in an exactly metastable droplet. The metastable droplet is therefore not an entirely appropriate context for checking the predictions of Nozières and Gallet for a static interface in the presence of an overpressure. Rather it illustrates the qualitative differences between an infinite planar surface and a finite curved surface under the same conditions.

However, one value of $F^*(T)$ is accessible for each system size L; specifically, for the set of parameters for which the system is approximately at the modified faceting transition. For the L=128 system shown in Fig. 6, this is at $T_R^* \simeq 0.450 T_c$. We can now check the prediction by examining Fig. 9: The data points are the empirically chosen overpressures (controlled by varying the undercooling of the liquid phase) for two system sizes (L=128 and 64) required for metastability. The solid line is the analytic prediction for $F^*(T)$ according to (14); it is the overpressure required to roughen a static surface at temperature $T < T_R$. The point of intersection indicates the trial temperature at which we expect to see the faceting transition in our data: it is in good agreement. It also indicates a shift in F^* related to system size which is consistent with our observations.

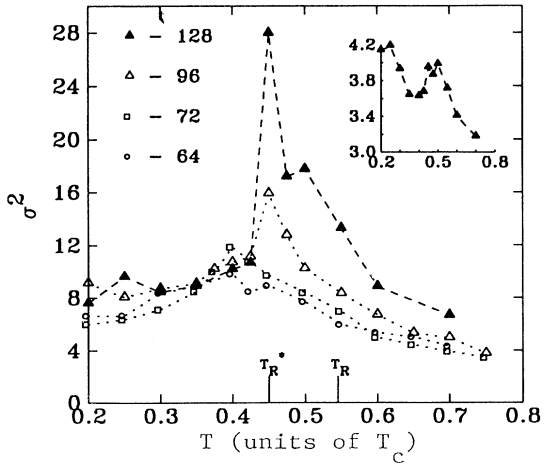

FIG. 8. The variance σ^2 of the mean microfacet area for the metastable droplet at $T \in [0.3T_c, 0.75T_c]$ for system sizes $L = 64, 72, 96$, and 128. The inset shows the mean microfacet area $\langle A \rangle$ for $L = 128$.

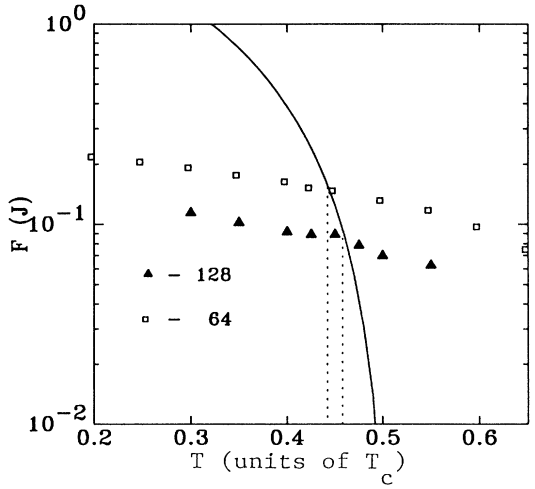

FIG. 9. The over pressures required for metastability at $T \in [0.2T_c, 0.65T_c]$ for system sizes $L = 64$ and 128 compared to the analytic prediction (solid line) of Nozières and Gallet, (14).

V. THE UNSTABLE DROPLET

Away from metastability, the droplet described in Sec. IV will tend to grow or shrink due to the imbalance between the overpressure and the surface tension. Since a growing droplet may be morphologically unstable, we will restrict our attention to the context of shrinking droplets at coexistence. We observe that the droplet is *forced* through a faceting transition to permit faster evaporation via a diffusion-limited process; we propose a description for this and predict the time dependence of the macrofacet radii and the droplet radius.

A. Theory

A droplet at coexistence, $T < T_R$ such that it would be faceted in the metastable state, is constituted of both faceted and roughened regions, each evaporating at disparate rates. As the roughened portions quickly evaporate, the curvature along the edges of the faceted regions becomes more pronounced; in the language of a curved-planar two-phase system, the phase-boundary energy between the curved and planar phases increases. Consequently, the system will try to further minimize its surface energy by reducing the size of the macrofacets. Far away from metastability, the faceted phase will be forced out of existence and the surface will assume a completely roughened state, *not due to the kinetic effects of the moving planar interface* but rather due to rapid evaporation of the adjoining roughened regions. If the droplet is close to metastability, the facets will only shrink slightly, reaching a nucleation-limited evaporation

regime where the faces remain faceted; for time scales which are much shorter than the activation time of the nucleated evaporation, the droplet behaves like the static droplet described in Sec. IV.

These two evaporation mechanisms have characteristic dynamical time dependences. In the diffusion-limited regime, as the solid gives way to the liquid and latent heat is absorbed to form the liquid, heat must be tranported from infinity to the interface. This is controlled by the diffusion constant D. Solving for the diffusion equation in radial coordinates for a sphere of radius R [23], the growth rate is shown to be

$$\frac{dR}{dt} = \frac{D}{R}\left(\triangle u - \frac{2d_0}{R}\right), \tag{15}$$

where $\triangle u \equiv (u_\infty - u)/u_\infty$ is the dimensionless undercooling from infinity, u is defined as

$$u \equiv \frac{T - T_m}{\lambda/c_p}$$

(λ is the latent heat of transition) and d_0 is the capillary length

$$d_0 \equiv \gamma T_m c_p/\lambda^2.$$

Note that this solution implies the *quasistatic approximation* where the time scale for thermal relaxation is much shorter than that for the interface dynamics; the diffusion constant D was chosen to satisfy this constraint. The $dR/dt = 0$ limit defines the critical droplet radius $R_c = 2d_0/\triangle u$ so that we can rearrange (15) and integrate it in the limit of small undercooling (i.e., the limit of $R_c \to \infty$), to give

$$R(t) = (R_0^3 - 6Dd_0t)^{1/3}. \tag{16}$$

By contrast, the behavior of the macrofacets is controlled by edge tension acting on their boundaries with the adjoining roughened regions. This is analogous to the *decay* of a 2D nucleation site which is smaller than the critical size $r_f < r_f^*$. If it is assumed that the adjoining regions are near local equilibrium (i.e., the time scale for their evaporation is much shorter than for the macrofacet dynamics), then we expect that the facets will shrink according to the Becker-Döring relation [24]; the volume of a droplet should decay at a rate proportional to its area $dV/dt \propto A$. For a near-circular 2D facet, the rate of evaporation then goes as the facet circumference, and we thus expect that $r_f(t)$ is linear in t.

To sum up, an evaporating, faceted droplet is expected to be limited by its facets, which shrink at a constant rate, until it becomes completely roughened. It will then be roughly spherical with a radius described by (16). It is expected that current experimental techniques should be able to observe this behavior on faceted crystals away from metastability. Certainly, independent measurements have been made of nucleation- and diffusion-limited growth [25] and evaporation on planar and droplet crystal interfaces [26–28]. In particular, the growth of crystals near equilibrium have been observed [29]; the crystals became strongly faceted with sharp edges. In contrast to the evaporation case, this appears as if the crystal is being forced into the completely faceted state. Although not presented here, this behavior has also been observed in our simulations.

B. Results

We ran several trials at the largest system size possible ($L = 128$) to minimize finite-size effects on the transition. The droplet was initialized as a cube of size $\ell = 0.75L$ at the ambient temperature $T = 0.3\ T_c$, with the liquid background also at T. The coexistence temperature T_m was also set to $0.3T_c$ so that the droplet completely evaporate (i.e., $R_c = \infty$). Except for local cooling at the surface due to the absorption of latent heat, the system was maintained at constant T via contact with a heat bath at the boundaries. The latent heat and diffusion rate were chosen such that the trial ended with the complete evaporation of the solid within 5000–50 000 MCS. The quantities r_f, $\langle A \rangle$, σ^2, and $\bar{m}$ (average system magnetization) were recorded; each gives a good indication of the transition of the cube surface from a faceted to a roughened state. Fig. 10 shows a time series of the evolution of a typical evaporating droplet.

Figure 11 shows the time-dependent facet radius $r_f(t)$

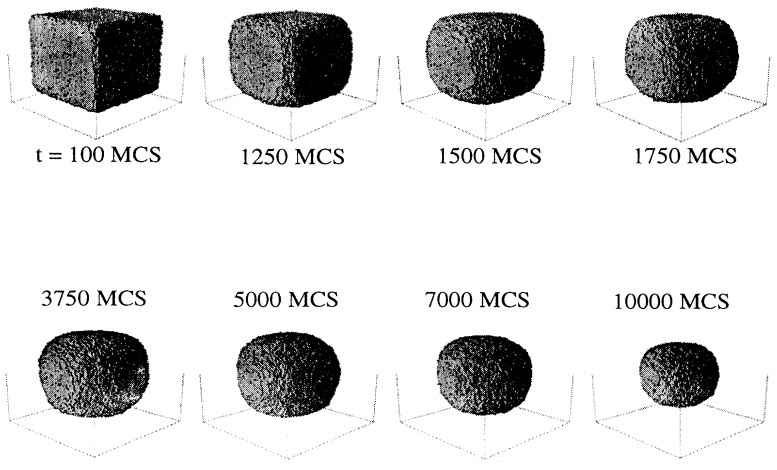

FIG. 10. Evolution of an unstable droplet as it evaporates from its initial cubic shape; the system is 128^3 with a 96^3 bulk inclusion at $T = 0.3T_c$. The transition from a faceted to a completely roughened state occurs at approximately $t = 5000$ MCS.

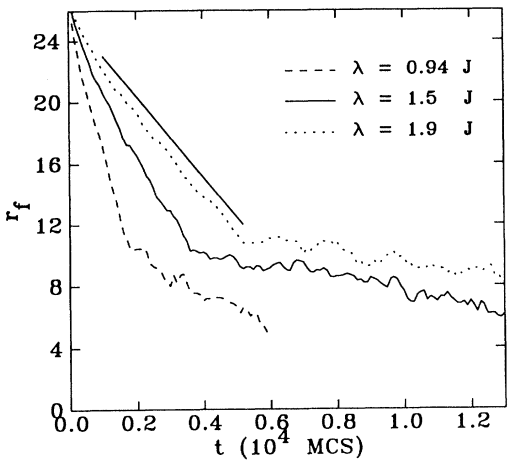

FIG. 11. The average macrofacet radius r_f as a function of time for unstable, evaporating droplets for system size $L = 128$ at $T = 0.3T_c$ for various values of the latent heat λ. The solid line illustrates the early-time linear behavior.

for several runs with differing latent heat; the transition from the faceted to roughened state is marked by a distinct change in slope. This is confirmed by a visual inspection of the cube surface; the entire time series of cube images is observed in a continuous playback, similar to a movie, and the point at which the the macrofacets disappear is selected as the time of transition. Further, total surface energy $E_{\rm tot}(t)$ and the moments of $P_f(t)$ have maxima at approximately the same transition point. Except for the first several hundred Monte Carlo steps before reaching local equilibrium, r_f is linear in t up to the transition point.

Figure 12 shows the time-dependent droplet radius $R(t)$. The disappearance of the macrofacets is marked by

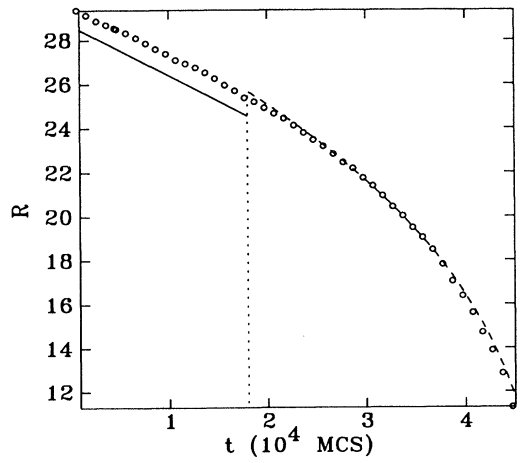

FIG. 12. The droplet radius R as a function of time for an unstable, evaporating droplet of size $\ell = 96$ at $T = 0.3T_c$; the dotted line indicates the transition from a faceted to a roughened state. The dashed line is a fit to the analytic expression (15) and the solid line illustrates the early-time linear behavior.

a change in the behavior of dR/dt. At early times, $R(t)$ appears to be linear in t, with droplet evaporation limited by the decay of the macrofacets. After the droplet is completely roughened, $R(t)$ can be fitted by the expression (16) and as a by-product the capillary length d_0 can be extracted for our choice of system parameters. We find $d_0 \simeq 0.378 \pm 0.002$ in units of lattice spacing.

VI. THE DRIVEN PLANAR INTERFACE

If an otherwise stable crystal interface is driven by an external force such that it has a steady-state behavior and a constant velocity, it may exhibit a *dynamic* or *kinetic* faceting transition. We have chosen to examine an undercooled planar {100} interface; the bulk free-energy difference between the *liquid* and *solid* phases provides a driving force which is limited by the diffusion of latent heat away from the interface. This case is of particular interest to us as it is representative of many crystal growth problems including our current studies of dendritic growth within the context of the Mullins-Sekerka instability [1,4]. Theoretical predictions [19] suggest that the dynamic faceting transition of the interface is broadened relative to the equilibrium behavior and that the effective T_R^* is depressed as a function of the interface velocity v. This is supported experimentally [30] and by other simulation studies [31]. The interface is expected to have a highly nonlinear response to a driving force while in a faceted state, compared to a nearly linear response when it roughens, due to the very different mechanisms responsible for the growth [17]. Although we will not be able to quantify the effect of the driving force, we will characterize it in terms of the variables defined in preceding sections.

A. Theory

At $T < T_R^*$ for a sufficiently small driving force, the interface moves via a nucleation process. Paraphrasing Nozières and Gallet [19], nucleation-limited growth is described in terms of microfacets which spontaneously appear as thermal fluctuations on the faceted surface at a rate $I \propto e^{-E_f/T}$. The energy of formation is now

$$E_f(\rho) = 2\pi\rho E_s - a\pi\rho^2 \triangle E_b$$

for a circular microfacet of radius ρ (ρ is expected to be larger than the lattice constant a); E_s and $\triangle E_b$ are the step free-energy and bulk free-energy difference, respectively. The critical microfacet radius (i.e., for $\rho > \rho_c$, they grow; otherwise, they decay) is $\rho_c = E_s/\triangle E_b$. This introduces a time scale for the creation of growing microfacets

$$1/\tau \propto e^{-E_f(\rho_c)/T}.$$

After time t, there will be on the order of t/τ microfacets, each growing with a lateral velocity v_ρ which is approximately constant in time. Since the edges of the microfacets are always rough (in 2D), the velocity is linearly dependent on the driving force [17]. The separation

between microfacets is

$$\eta \sim \rho_c \sqrt{\tau/t};$$

thus, they will join to form a new reference plane when $\rho\ (=v_\rho t) \sim \eta$. This defines the forward velocity of the interface $v \equiv a/t$ as

$$v \propto \left(\frac{\triangle E_b^2}{E_s}\right)^{2/3} e^{-\pi E_s^2/3\triangle E_b T}, \tag{17}$$

where a is the lattice spacing. The kinetic roughening transition occurs when the fluctuation correlation length is on the order of the critical microfacet size $\xi \sim \rho_c$; this condition is equivalent to the expression (14).

At $T > T_R^*$, the interface is roughened and growth is diffusion limited. The growth velocity is expected to depend approximately linearly on the driving force $F \equiv \triangle E_b \simeq \triangle T$ and should vary only with T for constant F.

B. Results

Our data refer to a {100} planar interface in a system of size 256 × 256 × 48, initialized at $T = 0.5T_c$. The driving force F is supplied through the bulk free-energy difference $\triangle E_b$ by varying the melting temperature T_m, and thus the *liquid* undercooling $\triangle T \equiv T_m - T$. The spin degeneracy is fixed at $\delta = 2.0$ and the ends of the system are maintained at T. Under these conditions, $\triangle E_b$ varies linearly with $\triangle T$. The *solid* is also initialized at T to minimize heating at the interface by allowing it to absorb some of the latent heat which is produced. The latent heat tends to heat both phases slightly, but temperatures are always maintained well below the equilibrium faceting transition temperature T_R. The undercooling is varied with $\triangle T \in [0.01T_c, 0.12\ T_c]$ and the simulations are run for 2000–10 000 MCS until steady state is reached; each data point is an average over one configuration (i.e., no time averaging). Figure 13 represents a series of driven planar interfaces at $T < T_R$.

Our first observation is that the experimental parameters such as A_0, $\langle A \rangle$, and σ^2 exhibit an oscillatory behavior related to the activated growth mechanism; the period is $\tau = a/v$, where a is the lattice unit and v is the interface velocity. For example, Fig. 14(a) shows A_0, the surface area of the reference plane, as a function of time for the slowest interface; A_0 has a minimum when the growing microfacets cover exactly half the reference plane and a maximum when the current reference plane has just finished forming. The quantities based on the microfacet distribution change in a similar manner; only a roughened plane will have a constant steady-state distribution. As the velocity of the interface increases with increasing driving force $\triangle T$, the period of the cycle decreases as shown in Figs. 14(b) and 14(c).

Figure 15 shows the velocity of the interfaces as a function of $\triangle T$ (closed triangles); the data are nonlinear and consistent with (17) up to $\triangle T \approx 0.04T_c$ where it then becomes linear. Also shown is the *reduced* velocity v/v_r (open circles). The reference velocity $v_r(\triangle T)$ is measured at a temperature above the equilibrium faceting

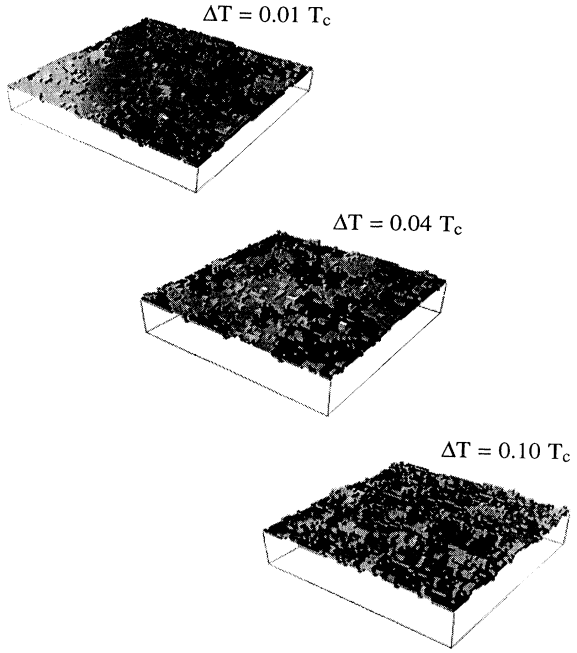

FIG. 13. Driven planar interfaces for a $64 \times 64 \times 48$ system at $T = 0.5T_c$ with under-coolings of $\triangle T = 0.02T_c, 0.04T_c$, and $0.1T_c$. The lighter grey indicates higher surface level. The equilibrium planar interface at $T = 0.5T_c$ in Figure 1 is the undriven equivalent of this interface.

temperature T_R where v_r is only dependent on the value of $\triangle T$. The reduced velocity clearly indicates that the effective dynamic transition is near $\triangle T^* \simeq 0.04T_c$.

Further evidence for this value comes from the character of the oscillations shown in Fig. 15. As the dynamic

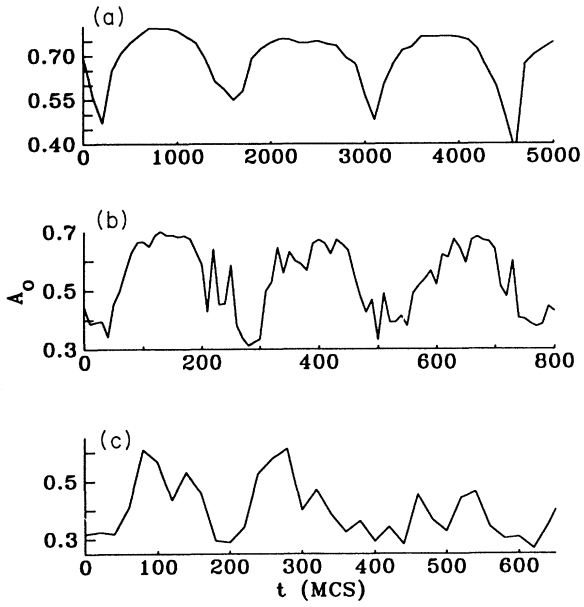

FIG. 14. The fractional area A_0 of the exposed reference plane for a driven equilibrium planar interface at $T = 0.5T_c$ for undercoolings of (a) $\triangle T = 0.02T_c$, (b) $0.04T_c$, and (c) $0.10T_c$. Note that the time scales for each plot are different.

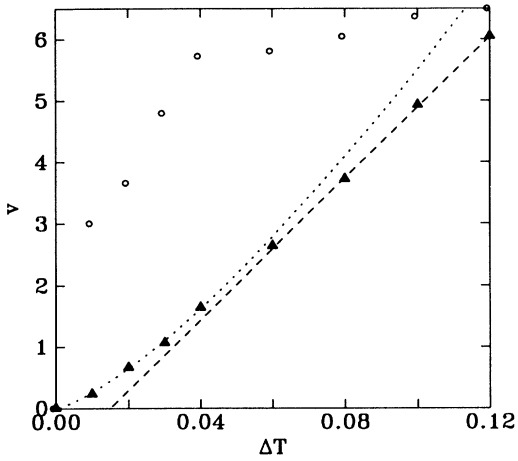

FIG. 15. The average interface velocity v (closed triangles) in units of lattice spacings per 1000 MCS for a driven steady-state planar interface at $T = 0.5T_c$ as a function of the undercooling ΔT. Also shown is the *reduced* velocity $v/v_r(\Delta T)$ (open circles). The dotted line indicates the analytic expression for v (17); the dashed line shows the high ΔT linear behavior.

roughening transition is approached, the smooth oscillations begin to break up. However, due to the broadened nature of the transition, oscillatory behavior is still observed at and above ΔT^*. This is consistent with the description of dynamical roughening near T_R^* offered by van Saarloos and Gilmer [32] wherein the interface is expected to be rough at long length scales but nucleated growth is still predominant at short length scales. Only near $\Delta T \simeq 0.12T_c$ does it appear that the interface has roughened at nearly all length scales.

The interface width $\langle w^2 \rangle$ does not exhibit any cyclic behavior except at the very lowest undercooling. Despite the changing microfacet distribution, $\langle w^2 \rangle$ is relatively smooth and relaxes to an average value once the thermal gradient reaches a steady state. Even in the case of $\Delta T = 0.01T_c$, the oscillatory behavior eventually damps out and $\langle w^2 \rangle$ reaches a steady-state value. Presumably this behavior is a reflection of the relatively large activation energy required for growth; when thermal fluctations are smaller than the critical fluctuation size, the growth may hesitate between layers. Figure 16 shows steady-state values of $\langle w^2 \rangle$ for various ΔT, showing a weak transition near $0.04T_c$; the inset shows a typical time evolution of the width of an interface.

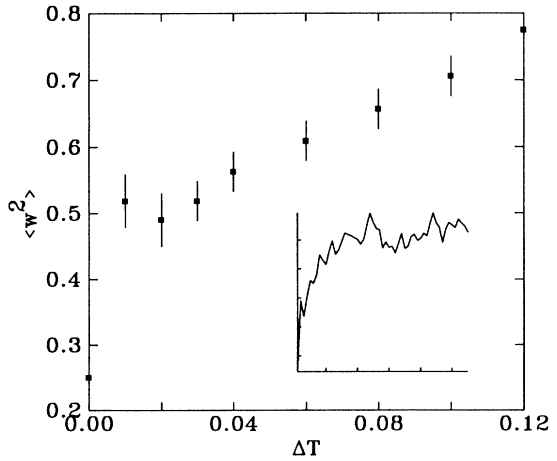

FIG. 16. The mean-squared width $\langle w^2 \rangle$ of a driven steady-state planar interface at $T = 0.5T_c$ as a function of undercooling ΔT. The inset shows the time-dependent width of a typical driven interface from an initially flat condition.

VII. CONCLUSIONS

In summary, we have simulated the faceting transition of a cubic crystal interface, at equilibrium and nonequilibrium and for planar and droplet geometries. We have introduced a method for characterizing a surface, and thus for identifying the transition, based upon the microfacet distribution. The approach works well in planar and nonplanar contexts where traditional methods are difficult to apply. The potential for use in nonequilibrium contexts is also evident.

Our results are consistent with other simulation studies in reproducing familiar critical behavior on the planar equilibrium interface. For a metastable droplet we observed the equilibrium crystal shape in accord with theoretical predictions. Our method clearly indicated the faceting transition and showed that the presence of a stabilizing external field had modified the transition behavior, depressing the effective transition temperature. Our measurement of the critical external field required to induce roughening at a specific temperature was in very good agreement with renormalization analysis. For the unstable droplet (with the stabilizing field removed), we simulated the relaxation to a roughened state from a faceted state and the subsequent evaporation of the droplet. Based on our observations, we proposed a mechanism to account for the decay of the macrofacets in the faceted phase and the decay of the droplet itself in both the faceted and roughened phases. Finally, we introduced a driving force in the form of a weak thermal gradient and observed the kinetic faceting transition for a planar interface at a temperature below the equilbrium transition temperature. We demonstrated the continued usefulness of our analysis technique, confirming the expected behavior of the transition, and noted the presence of a oscillatory behavior in the interface above and below the transition.

We see this work as a preliminary step in the study of the various structural transitions on a crystal surface. We intend to develop and expand it, especially with regard to the kinetic transitions, in the hope of making closer contact with experimental studies. We also plan to extend our simulations to other crystal lattices such as *hexagonal close packed*, where multiple transitions are observed experimentally [25, 33, 34].

ACKNOWLEDGMENTS

We are grateful to Martin Grant and Ken Elder for careful readings of the manuscript. Funding for the

project was from the NSERC of Canada and from le Fonds pour la Formation des Chercheurs et l'Aide à la Recherche de la Province du Québec.

APPENDIX

For convenience, in this appendix, we derive an expression for the mean curvature $\bar{\kappa}$ of a discrete interface, and relate this to the mean facet area $\langle A \rangle$.

If the interface is at thermodynamic equilibrium and is single valued $h(\mathbf{x})$, then the Fourier spectrum of modes has the form [16]

$$\langle |\tilde{h}(\mathbf{q})|^2 \rangle = \langle |\mathcal{F}(h(\mathbf{x}))|^2 \rangle \propto \frac{T}{\gamma(T) q^2},$$

where γ is the surface tension and $\mathcal{F}$ signifies a Fourier transform

$$\tilde{h}(\mathbf{q} \equiv \mathcal{F}(h(\mathbf{x})) = \int d\mathbf{x}\, e^{i\mathbf{q}\cdot\mathbf{x}}\, h(\mathbf{x}).$$

When the local curvature κ is small ($\nabla^2 h \ll 1$) then

$$\begin{aligned} \bar{\kappa}^2 = \langle \kappa^2 \rangle \cong \langle (\nabla^2 h)^2 \rangle &= \mathcal{F}^{-1}(\langle |q^2 \tilde{h}(\mathbf{q})|^2 \rangle) \\ &= \int_{2\pi/L}^{2\pi/a} d\mathbf{q}\, q^4 \langle \tilde{h}(\mathbf{q}) \tilde{h}(\mathbf{q})^* \rangle \\ &\approx \frac{T}{3} \left(\frac{2\pi}{a} \right)^3 \quad (L \gg a) \end{aligned} \tag{A1}$$

so that

$$\bar{\kappa} \propto \sqrt{T}. \tag{A2}$$

To relate $\bar{\kappa}$ to the area of the local microfacet A, we show in Fig. 17 the relationship of the interface to the underlying lattice with unit vector a. We choose a microfacet whose center is approximately contingent with the apex of the curved interface, and define its size l to be the solution of the expression

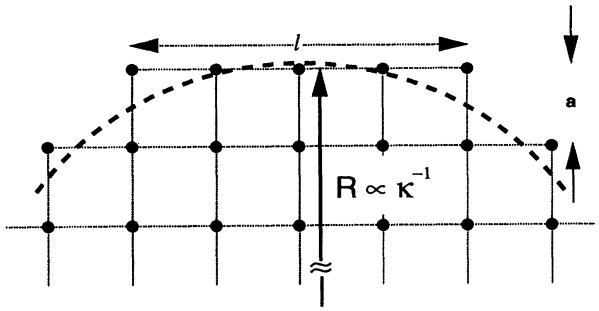

FIG. 17. Curvature of a discrete interface; see text.

$$\Delta h = h(\mathbf{x}) - h(\mathbf{x}_0) = \frac{1}{2} \kappa x^2 \equiv a.$$

The distance from edge to edge is therefore

$$l = 2\|\mathbf{x} - \mathbf{x}_0\| = 2\sqrt{2a/\kappa},$$

where Δh is assumed to be one lattice constant a. The microfacet area is then

$$A(\kappa) = l(\kappa)^2 = 8a/\kappa, \tag{A3}$$

so that, using (A2), the mean microfacet area behaves like

$$A(T) \propto T^{-1/2}, \quad T > T_R.$$

[1] R. Harris, L. Jörgenson, and M. Grant, Phys. Rev. A **45**, 1024 (1992).
[2] L. Jörgenson, R. Harris, and M. Grant, Phys. Rev. Lett. **63**, 1693 (1989).
[3] R. Harris and M. Grant, Phys. Rev. B **38**, 9323 (1988).
[4] L. Jörgenson, R. Harris, M. Grant, and H. Guo, Phys. Rev. E **47**, 1235 (1993).
[5] G.S. Pawley, R.H. Swendsen, D.J. Wallace, and K.G. Wilson, Phys. Rev. B, **29**, 4030 (1984).
[6] R. Harris, Phys Lett. **111**, 299 (1985).
[7] M. Creutz, Phys. Rev. Lett. **50**, 1411 (1984).
[8] M. Creutz, Ann. Phys. (N.Y.) **167**, 62 (1986).
[9] J.M. Kosterlitz, J. Phys. C **7**, 1046 (1974).
[10] R.H. Swendsen, Phys. Rev. B **25**, 2019 (1981).
[11] R.H. Swendsen, Phys. Rev. B **17**, 3710 (1978).
[12] S.T. Chui and J.D. Weeks, Phys. Rev. B **14**, 4978 (1976).
[13] K.K. Mon, D.P. Landau, and D. Stauffer, Phys. Rev. B **42**, 545 (1990).
[14] M. Holzer and M. Wortis, Phys. Rev. B **40**, 11 044 (1989).
[15] J. Adler, Phys. Rev. B **36**, 2473 (1987).
[16] M. Grant, Phys. Rev. B **37**, 5705 (1988).
[17] J.D. Weeks and G.H. Gilmer, in *Advances in Chemical Physics*, edited by I. Priogogine and S.A. Rice (Wiley, New York, 1979), Vol. 40, p. 157.
[18] M.E. Fisher, J. Phys. Soc. Jpn. **26**, 87 (1969).
[19] P. Nozières and F. Gallet, J. Phys. (Paris) **48**, 353 (1987).
[20] P. Nozières, J. Phys. (Paris) **50**, 2541 (1989).
[21] C. Rottman and M. Wortis, Phys. Rev. B **24**, 6274 (1981).
[22] M. Holzer, Phys. Rev. Lett. **64**, 653 (1990).
[23] J.S. Langer, Rev. Mod. Phys. **52**, 1 (1980).
[24] R. Becker and W. Döring, Ann. Phys. (Leipzig) **24**, 719 (1935).
[25] F. Gallet, S. Balibar, and E. Rolley, J. Phys. (Paris) **48**, 369 (1987).
[26] A. Dougherty and J.P. Gollub, Phys. Rev. A **38**, 3043 (1988).
[27] J.C. Heyraud and J.J. Métois, J. Cryst. Growth **50**, 571 (1980).
[28] J.J. Métois and J.C. Heyraud, J. Cryst. Growth **57**, 487 (1982).
[29] J.C. Heyraud and J.J. Métois, J. Cryst. Growth, **82**, 269 (1987).
[30] S. Balibar, F. Gallet, and E. Rolley, J. Cryst. Growth **99**, 46 (1990).
[31] B. Grossman, H. Guo, and M. Grant, Phys. Rev. A **43**, 1727 (1991).
[32] W. van Saarloos and G.H. Gilmer, Phys. Rev. B **33**, 4927 (1986).
[33] E. Rolley, S. Balibar, and F. Gallet, Europhys. Lett. **2**, 247 (1986).
[34] P.E. Wolf, S. Balibar, and F. Gallet, Phys. Rev. Lett. **51**, 1366 (1983).

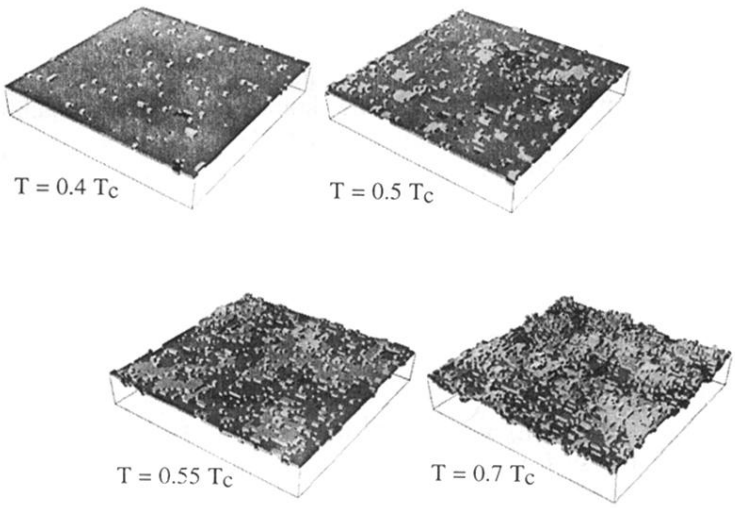

FIG. 1. Equilibrium planar interfaces for a $64 \times 64 \times 24$ system at $T = 0.4T_c, 0.5T_c, 0.55T_c$, and $0.7T_c$. The lighter grey indicates higher surface level.

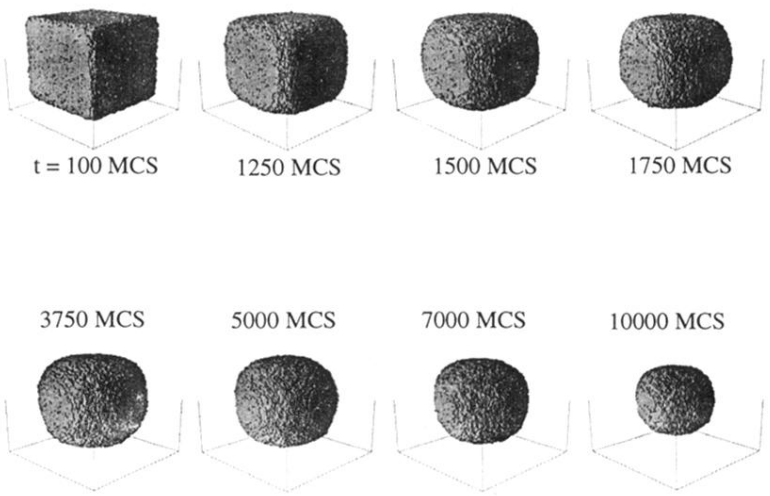

FIG. 10. Evolution of an unstable droplet as it evaporates from its initial cubic shape; the system is 128^3 with a 96^3 bulk inclusion at $T = 0.3T_c$. The transition from a faceted to a completely roughened state occurs at approximately $t = 5000$ MCS.

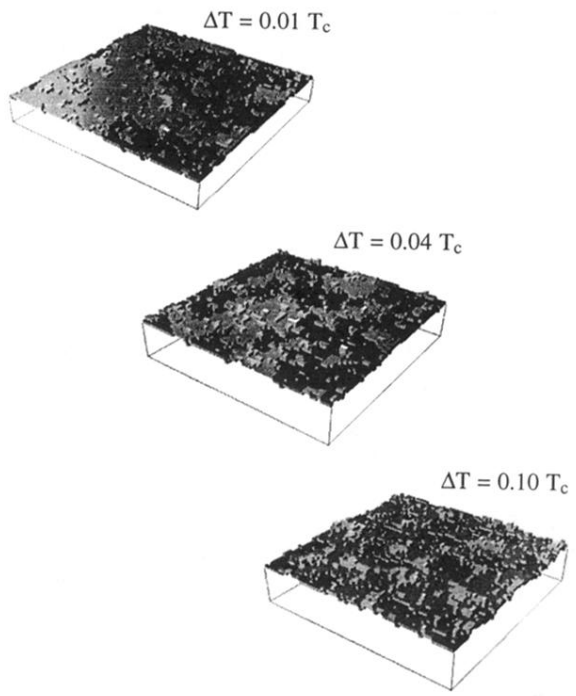

FIG. 13. Driven planar interfaces for a $64 \times 64 \times 48$ system at $T = 0.5T_c$ with under-coolings of $\Delta T = 0.02T_c, 0.04T_c$, and $0.1T_c$. The lighter grey indicates higher surface level. The equilibrium planar interface at $T = 0.5T_c$ in Figure 1 is the undriven equivalent of this interface.

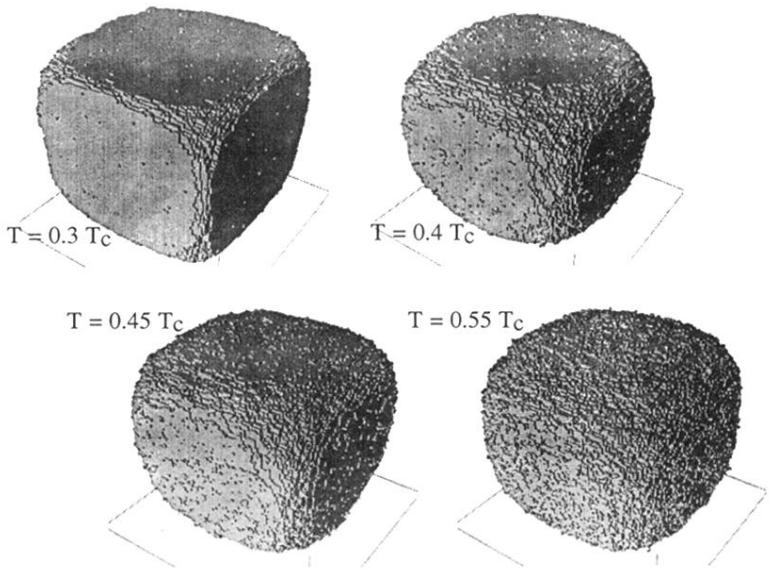

FIG. 6. Metastable interfaces for droplets of size 96^3 in a 128^3 system at temperatures $T = 0.3T_c, 0.4T_c, 0.45T_c$ and $0.55T_c$, near the modified faceting transition temperature $T_R^* \approx 0.45T_c$.